Chemical Vapor Deposition of Helical Carbon Nanofibers

Yoshiyuki Suda

Additional information is available at the end of the chapter

Abstract

Helical carbon nanofibers (HCNFs), including carbon nanocoils (CNCs), carbon nanotwists, and multi-walled CNCs, can be synthesized by chemical vapor deposition (CVD). HCNFs are predicted to have a high mechanical strength and hence are expected to have a use in nanodevices such as electromagnetic wave absorbers and sensors. For nanodevice applications, it is necessary to synthesize HCNFs in high yield and purity. In this chapter, I focus on CNCs and describe its history, expected application, and synthesis method. Finally, I introduce the author's recent studies on the improvement of the purity of CNCs by improving CVD conditions. A CNC layer with a thickness of larger than 40 μm was grown from a triple layer of $SnO_2/Fe_2O_3/SnO_2$ catalyst on a substrate, and the CNC purity increased to $81 \pm 2\%$.

Keywords: helical carbon nanofibers, carbon nanocoils, electromagnetic wave absorber, sensing devices, energy devices, binary catalyst, tetramethyltin, ferrocene, iron oxide fine powder

1. Introduction

1.1. Helical carbon nanofibers and carbon nanocoils

Carbon is an element with various allotropes because of its variety of chemical bonding: sp^1, sp^2, and sp^3. If we classify each carbon nanomaterial by its dimension, fullerene is a zero-dimensional substance, carbon nanotube (CNT) is a one-dimensional substance, and graphene is a two-dimensional substance. Helical carbon nanofiber (HCNF) is a helical-shaped carbon nanofiber with coil and fiber diameters in the range of 20–1000 nm and 5–400 nm, respectively. HCNFs are recognized as a three-dimensional substance according to the above definition.

There are two types of HCNFs: the first type, called CNCs, has an inner diameter and the second type does not have an inner diameter, and it is called carbon nanotwists. CNCs are classified into two types by their size and crystalline structure: CNCs and multi-walled CNCs (or coiled CNTs) which are the multi-walled CNTs with a coil geometry. In this chapter, I focus on CNCs (**Figure 1(a)**).

1.2. History

As far as I know, Davis et al. are the group who discovered CNCs. They have found minute vermicular growths of carbon through the experimental work on the deposition of carbon in the brickwork of blast furnaces in 1953 [1]. Two years later from the discovery, Hofer et al. reported the growth of carbon filaments with fiber diameters of 10–200 nm. They also found that the filaments were extended in two directions from central catalyst particles [2]. They used a catalytic chemical vapor deposition (CVD) technique of carbon from carbon monoxide.

After a while, Baker et al. developed a catalytic CVD using C_2H_2 gas over catalyst surfaces and studied the effect of Sn on the growth of filaments from the Fe/C_2H_2 system. They found that almost all the filaments had a spiral shape with a constant pitch and the Fe/Sn alloy worked to form spiral filaments [3, 4]. At the same time as Bakers' study, Boehm developed a continuous process of carbon filaments by feeding metal carbonyl into a CO stream before it passed a heated tube. He found that double or even triple helices were formed in the twisted filaments [5].

Carbon nanomaterials have been discovered one after another since the 1980s. Although fullerene [6], CNT [7], and carbon nanohorn (CNH) [8] were firstly synthesized by an arc discharge, CVD became a dominant technique in the research of carbon nanomaterials including HCNFs. In 1990, Motojima et al. have grown regularly coiled carbon filaments with a coil diameter of several micrometer by a catalytic CVD at 350–750°C using C_2H_2 gas feedstock and Ni as a catalyst [9]. Concurrently, Ivanov et al. have grown multi-walled CNC (or coiled CNT) which has a hollow structure with several concentric graphitic layers [10]. The CVD of single-walled CNTs (SWCNTs) was successfully realized in 1998 [11].

It is commonly accepted in CVD process that hydrocarbon precursors dissociate on catalyst particles, and the formed carbon species dissolve into catalyst particles and recombine to form carbon filaments. Models have been proposed to explain the formation of a helical structure in CNCs. Baker et al. postulated a bulk-diffusion model of carbon through catalyst particles based on the temperature gradient through a catalyst particle [3]. Another model was proposed by Amelinckx et al. and Fonseca et al. [12, 13]. The mismatch between extrusion velocities of different faces of a catalyst particle results in the deformation of carbon deposits.

1.3. Expected applications

Because of the structure of a solenoid coil, the application of electromagnetic wave absorber using CNCs [14–18] has been studied for the longest as an application of CNC. This is an application as a structural material with excellent electromagnetic wave absorption characteristics by mixing CNC with resin. It is comparatively easy and feasible for CNC application.
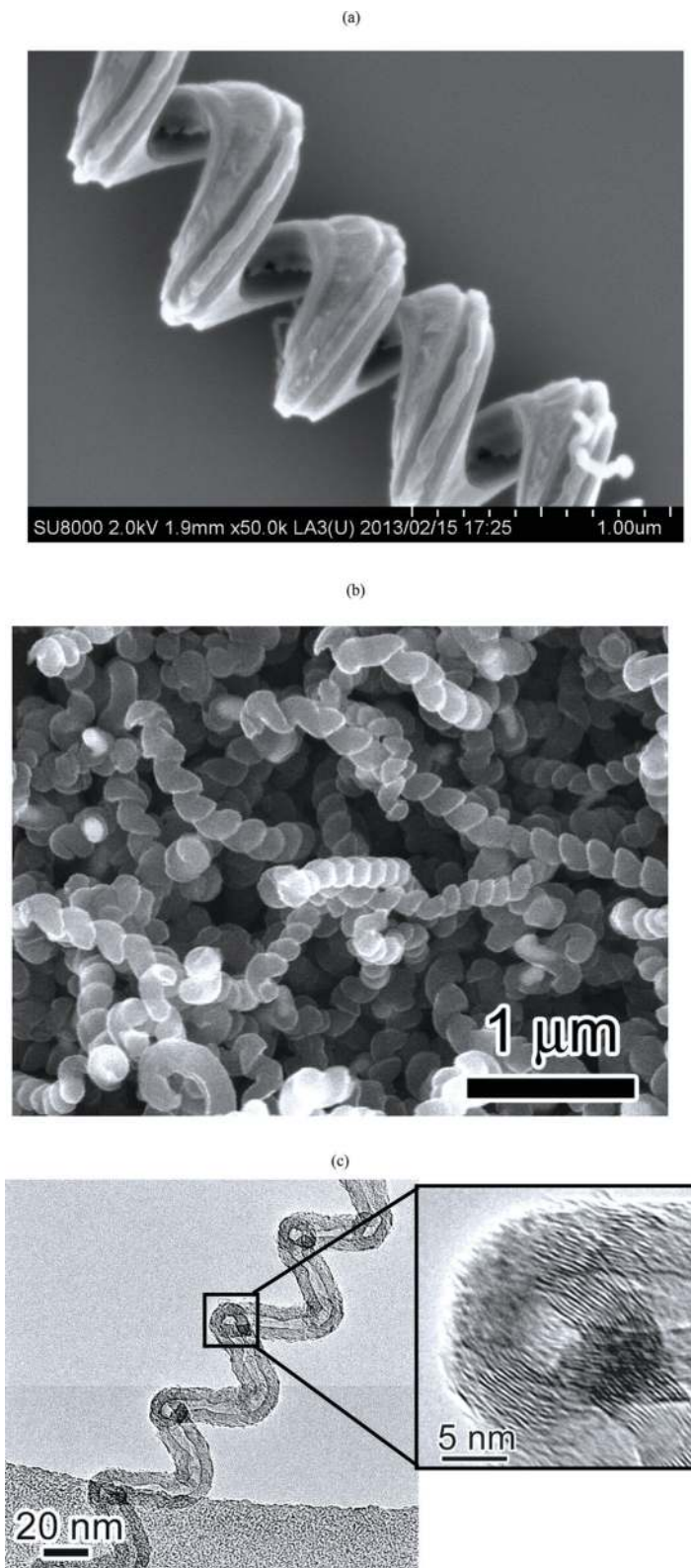
Figure 1. Scanning electron micrograph of HCNFs: (a) CNC, (b) carbon nanotwist, and (c) multi-walled CNC.

As a similar example, there is a fabrication of a sensing device in which plural CNCs are randomly integrated [19]. CNC-based biosensors [19], thermal sensors [20], and pressure and strain sensors [21–23] are reported one after another, and further development is expected.

On the other hand, there is no movement to use a single CNC as a nanospring or a nanoinductor, and it remains within the scope of basic research that it measures the spring constant [24] and estimates the inductance by simulation [25]. This is considered to be attributable to the fact that it takes a lot of trouble to arrange a single CNC in a desired place and direction and suitable application is not developed.

I am currently paying attention to the application of CNC to energy devices such as fuel cells [26–32] and electric double layer capacitors [33–37]. In this field, although carbon black and activated carbon, whose mass-production processes have been established, are used as a major carbon material, the applications of carbon nanomaterials including CNCs are progressing little by little. It is difficult at present to produce CNC at the same cost as these materials; its electrochemical properties higher than existing materials are however reported at the laboratory level. Future application of CNC is greatly expected.

2. Growth method

As fullerenes and CNTs were initially synthesized in high density plasmas such as laser vaporization and arc discharge, plasma processes have been used for synthesis of carbon nanomaterials. Meanwhile, CVD method is the mainstream of CNC since it was introduced in the 1970s. From the viewpoint of the carbon species to be supplied as a raw material, the method using plasma and the CVD method are summarized; a major difference is in between atomic and/or molecular carbon and hydrocarbon molecules.

Most hydrocarbons and alcohols are gaseous or liquid at ordinary temperature and normal pressure and can be easily introduced into the reaction furnace by using differential pressure or carrier gas. The hydrocarbon molecules supplied into the reactor are thermally decomposed by the catalytic reaction to change to the desired carbon nanomaterial. This process is called CVD method. Since synthesis of CNC by CVD method has much in common with synthesis of CNT, synthesis of CNT will be described first. As common to both materials, it is very important to arrange the supply of carbon feedstock and the synthesis site: catalyst and substrate.

In 1998, Dai's group succeeded in synthesizing single-walled CNTs by fixing Fe_2O_3 nanoparticles on a substrate and using CH_4 gas as a raw material [11]. This is explained by that hydrocarbon molecules are decomposed on the surface of Fe nanoparticles reduced in a high-temperature CH_4 atmosphere, carbon dissolves inside the nanoparticles (or diffuses on the surface), and carbon segregates from the nanoparticles to form CNT. This concept is basically the same as the synthesis process of carbon fiber, which was known before the discovery of CNTs [38]. Dai's group realized the growth of single-walled CNTs by maintaining the size of Fe nanoparticles to a minimum. On the other hand, in the synthesis of graphene, Cu in which the solubility of carbon is low is used as a catalyst. In this way, new catalysts have been developed.

Now, in order to synthesize CNC, the element which does not dissolve carbon inside such as Sn is mixed with Fe. The author tried various binary catalysts and showed that CNC can be synthesized from Fe/Sn catalyst with high efficiency [39]. Pan et al. synthesized CNC with high efficiency using a mixed catalyst of Fe and indium tin oxide (ITO) and proposed a model that the coil shape is formed due to the nonuniformity of the segregation speed of carbon from the catalyst nanoparticles [40]. There are several catalysts suitable for CNC growth, and there is a possibility that new combinations can be found in the future.

3. Recent improvement on CNC growth technique

It is now possible to produce 2–3 g of HCNFs on a catalyst-supported graphite substrate within an hour, using C_2H_2 feedstock [39]. However, problems of low CNC purity remain. The main problem of CNC synthesis is that CNCs can grow with high purity on the surface of carbon deposits, but interlayers with very low CNC purity are present inside the carbon deposit [39, 41, 42]. Here I introduce two techniques to improve CNC purity in CVD and the evaluation method of CNC purity. The CNC purity in most reports was evaluated by observing the surface of the carbon deposit. The variations in the CNC purity inside carbon deposits have not been yet understood completely.

3.1. Supplying catalyst molecules from the vapor phase

In this study, the Sn/Fe catalysts were supplied using the following four materials: a thin Sn film, a drop-coated solution of Fe_2O_3, tetramethyltin (TMT) vapor, and ferrocene vapor. The CNC purity averaged over the overall carbon deposit was increased 1.5-fold by the TMT supply. A maximum CNC purity of 72% using a combination of TMT and ferrocene vapors was obtained, with Sn/Fe deposition on the substrate [43].

Various experimental methods have been proposed for the production of high-purity CNCs [44–47]. However, the supply of vapor-phase catalysts during the synthesis of CNCs has been reported in only a few previous studies [48, 49]. In this study, we performed experiments in which different catalyst metal vapors were supplied successively in a CVD reactor.

3.1.1. Experimental setup and procedure

The experiments were performed in a horizontal CVD reactor using the following steps: (1) vacuum-evaporating Sn on the SiO_2/Si substrate, (2) drop-coating an Fe_2O_3 solution on the Sn-coated SiO_2/Si substrate and performing calcination, (3) mounting the Sn/Fe-coated SiO_2/Si substrate in the CVD reactor, (4) performing CVD using a C_2H_2/N_2 gas mixture, and (5) investigating the effects of changing the catalytic vapor supply, adding tetramethyltin (TMT) and/or ferrocene to C_2H_2/N_2 gas mixture during CVD.

Sn and Fe vapor catalysts were introduced into the CVD reactor using a tube pump and a vaporizer. TMT ($Sn(CH_3)_4$, purity: >96%, CAS No.: 594–27-4, Tokyo Chemical Industry Co., Ltd., Tokyo, Japan) and ferrocene ($Fe(C_5H_5)_2$, purity: > 95%, CAS No.: 102–54-5, Tokyo

Chemical Industry Co., Ltd., Tokyo, Japan) were used as the feedstocks for the Sn and Fe catalytic vapors, respectively. These catalyst molecules were mixed in ethanol, supplied to a vaporizer via a tube pump, and vaporized in a vaporizer. The CVD experimental conditions and catalytic vapor supply conditions are listed in **Tables 1** and **2**.

The synthesized CNCs and the catalyst nanoparticles were observed using SEM (S-4500II and SU8000, Hitachi High-Technologies Corp., Tokyo, Japan). The CNC purity was evaluated by analyzing SEM images of (1) the top surface and (2) the cross section of the samples. The carbon deposit was solidified by dropping a Nafion® solution onto the samples; then, the carbon deposit was cut to observe the cross section.

3.1.2. Results and discussion

In the experiment, the Fe catalyst was formed on the substrate before CVD and TMT vapors were supplied during CVD. The authors confirmed the growth of CNCs in all of the TMT concentration conditions (0.1–2% in ethanol) used in this study. The CNC number density was evaluated from the SEM images obtained at each TMT concentration, as shown in **Figure 2**. The CNC number density was highest at a TMT concentration of 0.2%. As the TMT concentration was higher than 0.2%, the CNC number density tended to decrease. The amount of carbon deposits showed the same tendency as the CNC number density.

By the above experimental results, the TMT concentration in ethanol was fixed at 0.2%, and the thickness of the Sn thin film was changed. CNC grew with all the Sn film thicknesses. Particularly, high-purity CNCs were obtained with the thicknesses of 40 and 60 nm. The CNC purity reached maximum (about 62%) for an Sn film thickness of 40 nm.

Figure 3 shows the as-grown carbon deposits on the substrate with a Sn film thickness of 40 nm and SEM micrographs of their cross sections. It was shown that the CNC purity inside

|	
Flow rates of C_2H_2/N_2 gases	50/1000 mL/min
Total gas pressure	1.013×10^5 Pa
Synthesis temperature	700°C
Growth time	30–600 s
Substrate	SiO_2/Si
Sn film thickness on substrate	0–60 nm
Amount of Fe_2O_3 solution (3% concentration) dropped on substrate	10 μL

Table 1. CVD conditions.

TMT concentration in ethanol	0.1–2%
Flow rate of TMT solution	0.144 mL/min
Temperature inside the carburetor	80°C

**Table 2.** Catalytic vapor supply conditions.
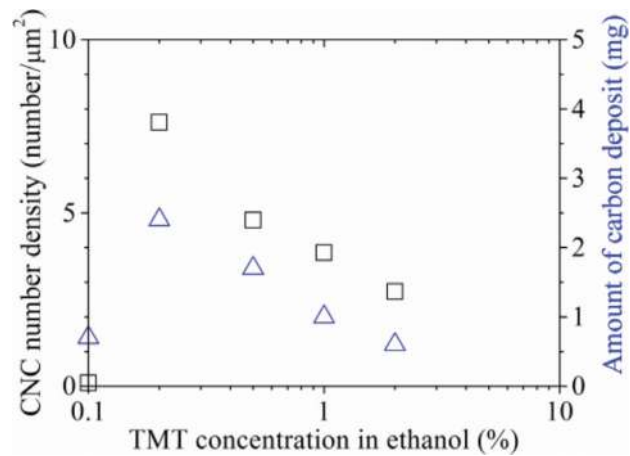
Figure 2. Dependence of the CNC number density (open squares) and amount of carbon deposits (open triangles) on the TMT concentration in ethanol. No Sn film was deposited on the SiO$_2$/Si substrates. The growth time was 600 s. The other growth conditions were the same as described in **Tables 1** and **2**.
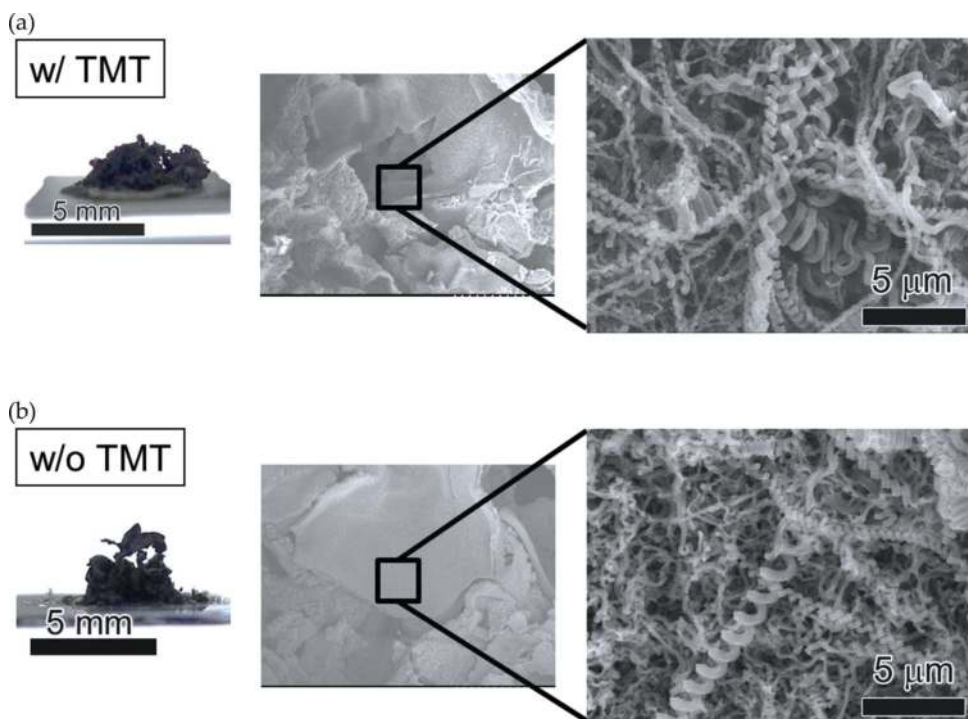
Figure 3. Photographs of as-grown carbon deposits and SEM micrographs of their cross sections: (a) with and (b) without TMT. The TMT concentration in ethanol, Sn film thickness, and growth time were 0.2%, 40 nm, and 600 s, respectively. The other growth conditions were the same as described in **Tables 1** and **2**.

the carbon deposit was lower than that of the surface from the SEM observation, regardless of TMT supply. The average CNC purities (average over the total carbon deposit) evaluated from the SEM image of the cross section of the carbon deposit were 42% for TMT and 28% without TMT. The CNC purity increased by 1.5 times by TMT supply. As shown in **Figure 4**, by the energy dispersive spectroscopy (EDS) analysis of the cross section of the carbon deposit,
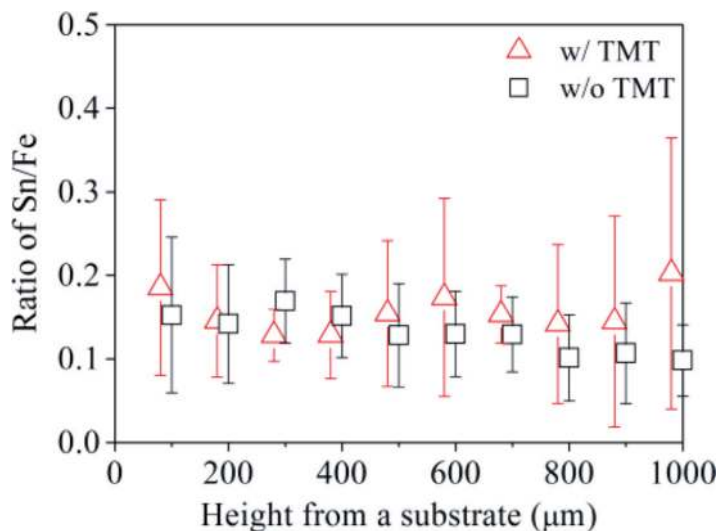
Figure 4. Relationship between the Sn/Fe ratio at the cross-sectional surfaces of the carbon deposits and the height from the substrate. The TMT concentration in ethanol, Sn film thickness, and growth time were 0.2%, 40 nm, and 600 s, respectively. The other growth conditions were the same as described in **Tables 1** and **2**.

every 100 μm from the substrate surface to a height of 1000 μm revealed that the molar ratio of Sn to Fe (Sn/Fe ratio) obtained with TMT supply was always higher than those without TMT supply. This suggests that Sn catalyst could be supplied by TMT to the interior of the carbon deposit as well as the substrate surface.

Next, the result of adding ferrocene to the TMT solution is explained. The molar ratio of Fe: Sn in the solution containing ferrocene was set to 3: 1. As shown in **Figure 5**, the CNC purity on the surface of carbon deposits obtained with different Sn film thicknesses was evaluated. It was clearly shown that the supply of ferrocene increases CNC purity. When the Sn film thickness was 40 nm, the purity of CNC reached a maximum (72%).
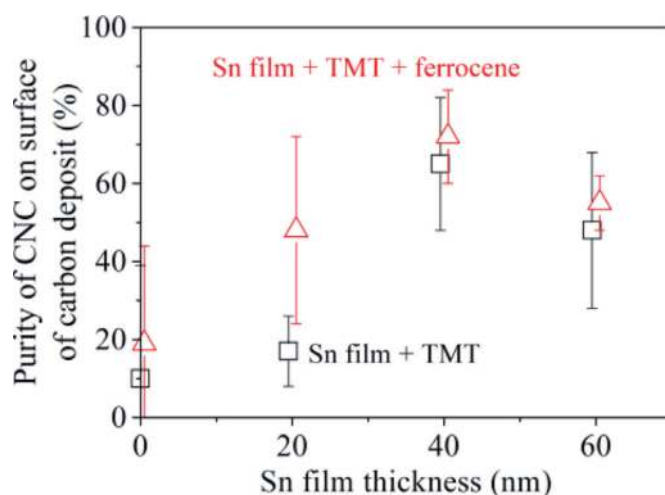
Figure 5. Purity of CNCs grown on the surface of carbon deposits under a supply of TMT and ferrocene. The TMT concentration in ethanol and growth time was 0.2% and 600 s, respectively. The other growth conditions were the same as described in **Tables 1** and **2**.

When ferrocene is added, not only Sn but also Fe is supplied as steam. Then, it is possible that these catalysts will grow CNC in the gas phase. In order to confirm this, carbon deposits on the inner wall of the CVD apparatus were analyzed after the CVD experiment. Several CNFs were observed by SEM, but the presence of CNC was not confirmed. Since ferrocene and TMT could be decomposed at the CVD growth temperature used in this study [50, 51], it seems reasonable that CNFs were grown from catalyst nanoparticles in the vapor phase. Li et al. however argue that it is necessary for the CNC catalyst nanoparticles to be fixed on a substrate to form the CNCs' helical structure [41].

3.2. Using iron oxide fine powder as a catalyst

In this section, the experimental results that increase the purity of CNC by improving the structure of the catalyst layer and CVD conditions are introduced [52]. By forming a triple-layer structure of $SnO_2/Fe_2O_3/SnO_2$ catalyst on the substrate and optimizing the CVD conditions, a CNC layer with a thickness of 40 μm or more was grown, and the CNC purity inside this layer successfully raised to $81 \pm 2\%$.

There is a carbon layer that does not contain CNCs between the upper and lower CNC layers; this was called the carbon layer. Both the CNC and carbon layers were grown from a catalyst that was deposited on the substrate. In the author's experiment, when this carbon layer was taken into account, the CNC purity over the whole deposits grown became almost 55%, very low compared to the purity of the CNC layer. Yokota et al. [39] reported that the thickness of the carbon layer depends on the thickness of the catalyst film on the substrate.

In order to increase the CNC purity and reduce the thickness of the carbon layer, formation of the catalyst layer by using a spin coating method and Fe fine powder was attempted. CNCs were synthesized using an automatic CVD apparatus.

### 3.2.1. Experimental setup and procedure

The CVD conditions in this study are listed in **Table 3**. The detail of the automatic CVD apparatus is described elsewhere [53].

In this experiment, the authors replaced a Fe powder (diameter: 1–3 μm) with a Fe fine powder (diameter: 20 nm) and used the spin coating method for coating Fe on the substrate in order to reduce the catalyst film thickness. Solution of Fe_2O_3 (0.1 M) and SnO_2 (0.13 M) was separately coated on the Si substrate. The spin coating speed was varied between 1000 rpm and 2500 rpm. After coating one kind of solution, the substrate was dried at 80°C for 5 minutes to suppress mixture of the solutions. The following three kinds of catalyst structures were formed: (a) Fe_2O_3/SnO_2, (b) SnO_2/Fe_2O_3, and (c) $SnO_2/Fe_2O_3/SnO_2$. By observing the catalyst structure with SEM, the optimum catalyst structure for CNC growth and the influence of this structure on the thickness of the carbon layer were investigated [52].

The purity of CNCs over the entire deposit was evaluated. As illustrated in **Figure 6**, the carbon deposit is sheet-like in shape, and CNCs were grown on both sides of the carbon layer.

Catalyst precursor	Fe_2O_3 fine powder (diameter: 20 nm, Nilaco, Tokyo, Japan)
	SnO_2 drop-coating solution (0.13 M, Kojundo Chemical Laboratory, Sakado, Japan)
Spin coating velocity	1000–2500 rpm
Catalyst structure	Fe_2O_3/SnO_2, $SnO_2/Fe_2O_3/SnO_2$, SnO_2/Fe_2O_3
Catalyst molar ratio	Fe:Sn = 1:2.6–1:13
Feedstock gas (flow rate)	C_2H_2 (100–400 mL/min)
Dilution gas (flow rate)	N_2 (1000–1800 mL/min)
Synthesis temperature	780°C
Synthesis time	0.5–30 min
Annealing temperature	780°C
Annealing time	5 min

Table 3. Catalytic CVD conditions.
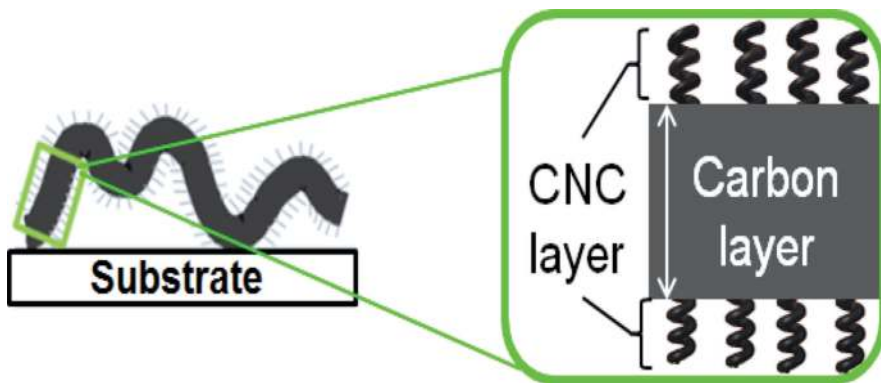
Figure 6. Illustration of the carbon deposit.

The CNC purity was defined by Eq. (1) under the assumption that the CNC purities in the CNC and the carbon layers are 100% and 0%, respectively.

$$CNC \ purity \ = \ \frac{Thickness \ of \ CNC \ layer}{Thicknesses \ of \ CNC \ and \ carbon \ layers} \times 100 \ (\%) \qquad (1)$$

The assumption is consistent with the SEM observations of the deposits. The thickness of the CNC layer was obtained as the summation of the upper and lower layers.

3.2.2. Results and discussion

Firstly, the effect of flow rates of C_2H_2 feedstock and N_2 dilution gases on CNC growth was examined. The conditions in this experiment are as follows: catalyst structure, triple layer ($SnO_2/Fe_2O_3/SnO_2$); Fe/Sn molar ratio, 1:2.6; spin coating velocity, 1000 rpm; and synthesis time, 10 min. The other conditions are the same as the conditions shown in **Table 2**. In the

experiment in which the gas flow rate was varied, the flow rate of C_2H_2 gas was fixed at 250 mL/min, and the flow rate of N_2 gas was varied. Similarly, the flow rate of C_2H_2 gas was changed by fixing the flow rate of N_2 gas to 1400 mL/min.

The thickness ratio of the CNC layer and the carbon layer was examined by changing the flow ratio between C_2H_2 gas and N_2 gas. As a result, the thickness of the CNC layer as well as that of the carbon layer was maximized with a C_2H_2/N_2 gas flow ratio of 0.18 and decreased when the C_2H_2/N_2 gas flow ratio was greater than 0.18. Also, the difference in thickness between the CNC and the carbon layer was maximized at a C_2H_2/N_2 gas flow ratio of 0.18. When the C_2H_2/N_2 gas flow rate ratio was in the range of 0.15–0.25, the purity of CNC in the CNC layer was 95% or more.

Then, the influence of the spin coating velocity was investigated. The experimental conditions different from the experiment of the gas flow rate dependence are as follows: catalyst structure on substrate, two layers (Fe_2O_3/SnO_2); C_2H_2 gas flow rate, 250 mL/min; and N_2 gas flow rate, 1400 mL/min. Other conditions are the same as those shown in **Table 2**. The thicknesses of the CNC layer and the carbon layer with respect to the spin coating velocity are shown in **Figure 7**. The thickness of the carbon layer decreased with increasing spin coating velocity. It is believed that the amount of liquid remained on the substrate was reduced by increasing the spin coating velocity from 1000 to 2500 rpm. Since the CNC layer was hardly formed at a spin coating rate of 1500 rpm or more, the upper limit of the spin coating velocity seems to be 1000 rpm. From the experimental results, the optimum spin coating velocity was 1000 rpm. At this velocity, the CNC purity became highest, but the thickness of the carbon layer was also highest.

The effect of synthesis time on CNC growth was also examined. As synthesis time increased from 30 s to 10 min, the CNC purity increased constantly. However, the CNC purity remained almost constant at 75% for synthesis times between 10 and 30 min, indicating saturation tendency.

Next, the influence of the catalyst structure on carbon deposition was investigated using three types of catalyst structures. Different conditions from the above two experiments are as follows: spin coating velocity, 1000 rpm and synthesis time, 30 min. Other conditions are the
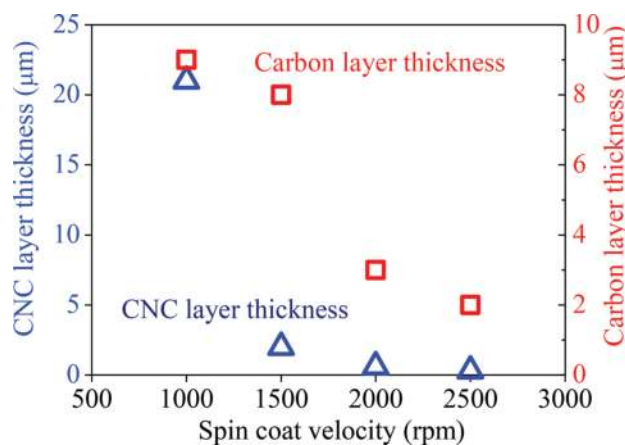

Figure 7. Thicknesses of CNC and carbon layers vs. spin coating velocity.

same as those listed in **Table 2**. Cross-sectional SEM micrographs of carbon deposits containing CNC and carbon layers grown from three types of catalyst structures and SEM micrographs of the surface of the CNC layers are shown in **Figures 8** and **9**, respectively.

As shown in **Figure 8**, a CNC layer was formed on the catalyst structures of (a) Fe_2O_3/SnO_2 and (b) SnO_2/Fe_2O_3/SnO_2. The purities of CNCs in (a) and (b) were estimated to be 69% ± 2% and 81% ± 2%, respectively, according to Eq. (1). The reason for that the CNC purity differs depending on the catalyst structure was examined using a CNC growth model as shown in **Figure 10**.
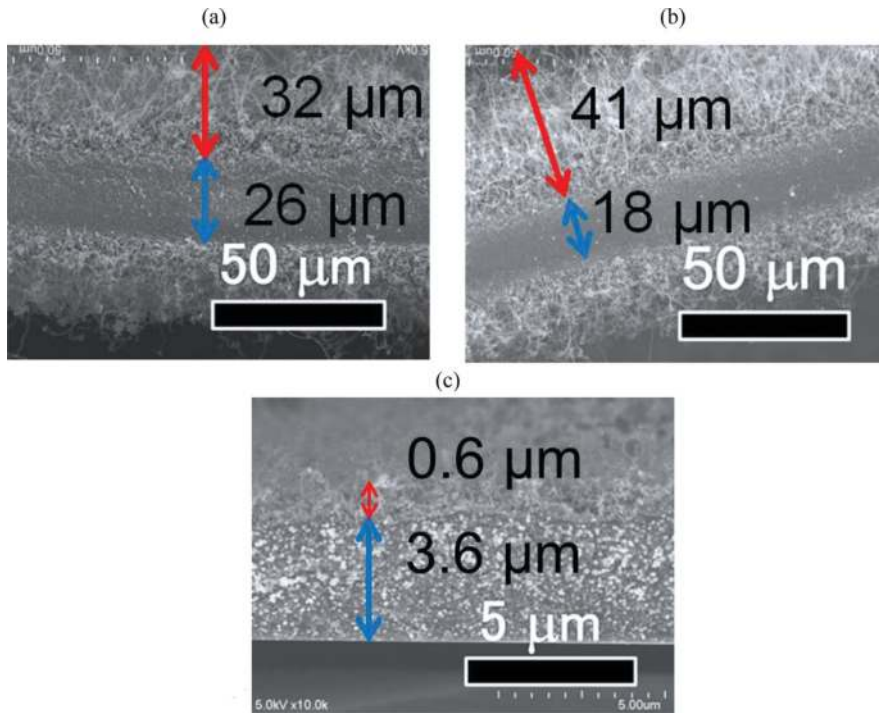
Figure 8. Cross-sectional SEM micrographs of carbon deposits grown with different catalyst structures: (a) Fe_2O_3/SnO_2, (b) SnO_2/Fe_2O_3/SnO_2, and (c) SnO_2/Fe_2O_3. The red and blue arrows represent the thicknesses of the CNC and carbon layers, respectively.
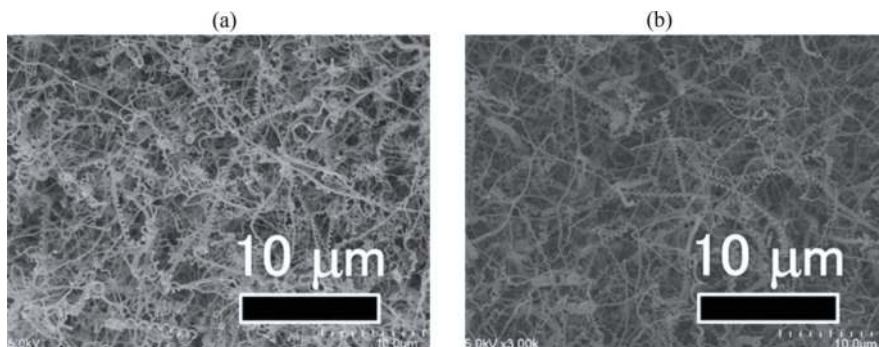
Figure 9. SEM micrographs of the surfaces of CNC layers grown from different catalyst structures: (a) Fe_2O_3/SnO_2 and (b) SnO_2/Fe_2O_3/SnO_2. No CNCs were observed on the SnO_2/Fe_2O_3 catalyst structure.
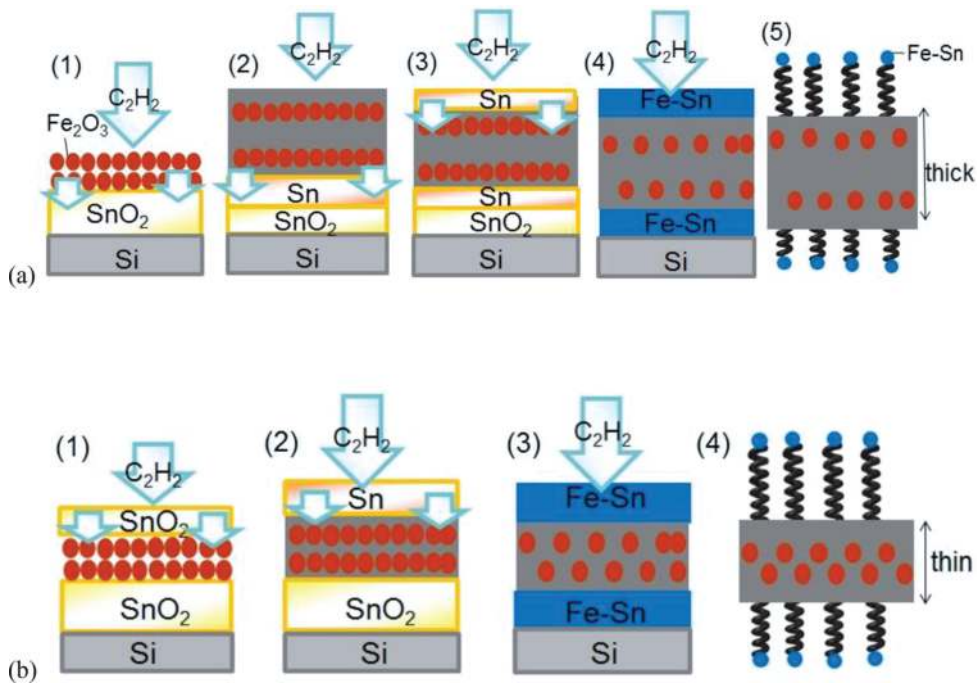
Figure 10. Growth models of (a) Fe_2O_3/SnO_2 and (b) SnO_2/Fe_2O_3/SnO_2 catalyst structures.

When C_2H_2 source gas molecule is supplied on the Fe_2O_3/SnO_2 catalyst, Fe_2O_3 in the catalyst forms nanoparticles ((1) in **Figure 10a**). A part of C_2H_2 molecule passes through the Fe_2O_3 to SnO_2, and SnO_2 is partially reduced by C_2H_2 molecules. Since the melting point of Sn is 232°C., which is much lower than the CVD temperature, a part of the reduced Sn stays as a liquid phase, and the other part diffuses inside the catalyst ((2) in **Figure 10a**). This phenomenon is explained by previous research results that molten Sn diffuses through the pores in the Fe_2O_3 thin film by capillary action [43]. However, since the amount of the Fe-Sn alloy formed on the surface of the Fe_2O_3/SnO_2 structure is limited ((3) in **Figure 10a**), a lot of sheets of carbon deposits are formed inside the Fe-Sn structure ((4) in **Figure 10a**). From the above, in the Fe_2O_3/SnO_2 catalyst structure, C_2H_2 molecules are directly supplied to Fe_2O_3 having a strong ability to decompose C_2H_2, and a very thick carbon layer is formed.

On the other hand, the amount of C_2H_2 molecules reaching the Fe_2O_3 catalyst nanoparticles in the SnO_2/Fe_2O_3/SnO_2 catalyst structure is limited ((1) in **Figure 10b**). By supplying more C_2H_2 molecules, an Fe-Sn alloy is formed on the upper and lower surfaces of SnO_2/Fe_2O_3/SnO_2, the same as in the case of the Fe_2O_3/SnO_2 catalyst structure ((3) in **Figure 10b**). However, the thickness of the layer is greater than the thickness of the layer formed from the Fe_2O_3/SnO_2 catalyst structure due to the much amount of Sn on the surface. Since CNC grows from the Fe-Sn alloy ((4) in **Figure 10b**), the thickness of the carbon layer grown inside the SnO_2/Fe_2O_3/SnO_2 catalyst structure becomes thinner than in the case of Fe_2O_3/SnO_2. This consideration explains the experimental results shown in **Figure 8**.

In the both models described above, the diffusion of C_2H_2 in the catalyst film is an important process for the growth of the CNC layer. This leads to a difference in thickness between the

upper and lower CNC layers. As the experimental results show, the thickness of the upper CNC layer was always thicker than the thickness of the lower CNC layer. This also explains the reason for that CNC hardly grows on the SnO_2/Fe_2O_3 catalyst structure. This indicates that when the SnO_2 layer is too thick, the amount of C_2H_2 supplied to Fe_2O_3 is appreciably limited. Based on the above experimental results, the authors concluded that the optimum catalyst structure for growing CNC in high yield and high purity is the $SnO_2/Fe_2O_3/SnO_2$ catalyst structure.

4. Summary

CNC, one type of HCNFs, is introduced. CNC has a coil diameter of 20–1000 nm, and a length of several tens of μm and has mainly been synthesized by a CVD method. Although it is very small, CNC is predicted to have a high mechanical strength and an electrical property and hence is expected to have a use in nanodevices such as electromagnetic wave absorbers and material in energy devices. The history, expected application, and synthesis method were described. The authors' recent studies on the improvement of the purity of CNCs by improving CVD conditions were summarized.

Acknowledgements

Conflict of interest

The author declares that he has no conflict of interest.

Author details

Yoshiyuki Suda

Address all correspondence to: suda@ee.tut.ac.jp

Toyohashi University of Technology, Toyohashi, Japan

References

[1] Davis WR, Slawson RJ, Rigby GR. An unusual form of carbon. Nature. 1953;**171**:756. DOI: 10.1038/171756a0

[2] Hofer LJE, Sterling E, McCartney JT. Structure of carbon deposited from carbon monoxide on iron, cobalt and nickel. The Journal of Physical Chemistry. 1955;**59**:1153-1155. DOI: 10.1021/j150533a010

[3] Baker R. Nucleation and growth of carbon deposits from the nickel catalyzed decomposition of acetylene. Journal of Catalysis. 1972;**26**:51-62. DOI: 10.1016/0021-9517(72)90032-2

[4] Baker RTK, Harris PS, Terry S. Unique form of filamentous carbon. Nature. 1975;**253**:37-39. DOI: 10.1038/253037b0

[5] Boehm HP. Carbon from carbon monoxide disproportionation on nickel and iron catalysts: Morphological studies and possible growth mechanisms. Carbon. 1973;**11**:583-590. DOI: 10.1016/0008-6223(73)90323-0

[6] Kroto HW, Heath JR, O'Brien SC, Curl RF, Smalley RE. C_{60}: Buckminsterfullerene. Nature. 1985;**318**:162. DOI: 10.1038/318162a0

[7] Iijima S. Helical microtubules of graphitic carbon. Nature. 1991;**354**:56-58. DOI: 10.1038/354056a0

[8] Iijima S, Yudasaka M, Yamada R, Bandow S, Suenaga K, Kokai F, et al. Nano-aggregates of single-walled graphitic carbon nano-horns. Chemical Physics Letters. 1999;**309**:165-170. DOI: 10.1016/S0009-2614(99)00642-9

[9] Motojima S, Kawaguchi M, Nozaki K, Iwanaga H. Growth of regularly coiled carbon filaments by Ni catalyzed pyrolysis of acetylene, and their morphology and extension characteristics. Applied Physics Letters. 1990;**56**:321-323. DOI: 10.1063/1.102816

[10] Ivanov V, Nagy JB, Lambin P, Lucas A, Zhang XB, Zhang XF, et al. The study of carbon nanotubules produced by catalytic method. Chemical Physics Letters. 1994;**223**:329-335. DOI: 10.1016/0009-2614(94)00467-6

[11] Kong J, Cassell AM, Dai H. Chemical vapor deposition of methane for single-walled carbon nanotubes. Chemical Physics Letters. 1998;**292**:567-574. DOI: 10.1016/S0009-2614 (98)00745-3

[12] Amelinckx S, Zhang XB, Bernaerts D, Zhang XF, Ivanov V, Nagy JB. A formation mechanism for catalytically grown helix-shaped graphite nanotubes. Science. 1994;**265**:635-639. DOI: 10.1126/science.265.5172.635

[13] Fonseca A, Hernadi K, Nagy Jb, Lambin P, Lucas AA. Model structure of perfectly graphitizable coiled carbon nanotubes. Carbon. 1995;**33**:1759-1775. DOI: 10.1016/0008-6223(95)00150-3

[14] Zhao D-L, Shen Z-M. Preparation and microwave absorption properties of carbon nanocoils. Materials Letters. 2008;**62**:3704-3706. DOI: 10.1016/j.matlet.2008.04.032

[15] Liu L, He P, Zhou K, Chen T. Microwave absorption properties of carbon fibers with carbon coils of different morphologies (double microcoils and single nanocoils) grown on them. Journal of Materials Science. 2014;**49**:4379-4386. DOI: 10.1007/s10853-014-8137-z

[16] Eguchi U, Takikawa H, Suda Y. Electromagnetic wave absorption characteristics of multiwalled carbon nanocoils. Japanese Journal of Applied Physics. 2014;**53**:045102. DOI: 10.7567/JJAP.53.045102

[17] Jian X, Chen X, Zhou Z, Li G, Jiang M, Xu X, et al. Remarkable improvement in microwave absorption by cloaking a micro-scaled tetrapod hollow with helical carbon nanofibers. Physical Chemistry Chemical Physics. 2015;**17**:3024-3031. DOI: 10.1039/C4CP04849K

[18] Li L, Lu L, Qi S. Preparation, characterization and microwave absorption properties of porous nickel ferrite hollow nanospheres/helical carbon nanotubes/polypyrrole nanowires composites. Journal of Materials Science: Materials in Electronics. 2018;**29**:8513-8522. DOI: 10.1007/s10854-018-8865-y

[19] Jia X, Hu G, Nitze F, Barzegar HR, Sharifi T, Tai C-W, et al. Synthesis of palladium/helical carbon nanofiber hybrid nanostructures and their application for hydrogen peroxide and glucose detection. ACS Applied Materials & Interfaces. 2013;**5**:12017-12022. DOI: 10.1021/am4037383

[20] Su C-C, Huang C-L, Chang S-H. Fabrication of aligned carbon nanocoil thermal sensor with a high temperature coefficient of electrical resistance at 25-100 °C. IEEE Transactions on Nanotechnology. 2015;**14**:794-797. DOI: 10.1109/TNANO.2015.2426611

[21] Li C, Pan L, Deng C, Wang P, Huang Y, Nasir H. A flexible, ultra-sensitive strain sensor based on carbon nanocoil network fabricated by an electrophoretic method. Nanoscale. 2017;**9**:9872-9878. DOI: 10.1039/C7NR01945A

[22] Deng C, Pan L, Zhang D, Li C, Nasir H. A super stretchable and sensitive strain sensor based on a carbon nanocoil network fabricated by a simple peeling-off approach. Nanoscale. 2017;**9**:16404-16411. DOI: 10.1039/C7NR05486F

[23] Li C, Pan L, Deng C, Cong T, Yin P, Wu Z. A highly sensitive and wide-range pressure sensor based on a carbon nanocoil network fabricated by an electrophoretic method. Journal of Materials Chemistry C. 2017;**5**:11892-11900. DOI: 10.1039/c7tc04166g

[24] Chen X, Zhang S, Dikin DA, Ding W, Ruoff RS, Pan L, et al. Mechanics of a carbon nanocoil. Nano Letters. 2003;**3**:1299-1304. DOI: 10.1021/nl034367o

[25] Wiselin J, Suseela SB, Jalaja BV, Ramani SDSP, Prasad R, Devaraj S, et al. A Low cost carbon nanofiber based spiral inductor: inference and implementation. Advances in Materials Science and Engineering. 2014;**2014**:1-8. DOI: 10.1155/2014/384917

[26] Park K-W, Sung Y-E, Han S, Yun Y, Hyeon T. Origin of the enhanced catalytic activity of carbon nanocoil-supported PtRu alloy electrocatalysts. The Journal of Physical Chemistry B. 2004;**108**:939-944. DOI: 10.1021/jp0368031

[27] Leela Mohana Reddy A, Jafri RI, Jha N, Ramaprabhu S, Ajayan PM. Carbon nanocoils for multi-functional energy applications. Journal of Materials Chemistry. 2011;**21**:16103. DOI: 10.1039/c1jm12580j

[28] Hu G, Nitze F, Sharifi T, Barzegar HR, Wågberg T. Self-assembled palladium nanocrystals on helical carbon nanofibers as enhanced electrocatalysts for electro-oxidation of small molecules. Journal of Materials Chemistry. 2012;**22**:8541. DOI: 10.1039/c2jm16075g

[29] Nitze F, Mazurkiewicz M, Malolepszy A, Mikolajczuk A, Kędzierzawski P, Tai C-W, et al. Synthesis of palladium nanoparticles decorated helical carbon nanofiber as highly active anodic catalyst for direct formic acid fuel cells. Electrochimica Acta. 2012;**63**:323-328. DOI: 10.1016/j.electacta.2011.12.104

[30] Suda Y, Shimizu Y, Ozaki M, Tanoue H, Takikawa H, Ue H, et al. Electrochemical properties of fuel cell catalysts loaded on carbon nanomaterials with different geometries. Materials Today Communications. 2015;**3**:96-103. DOI: 10.1016/j.mtcomm.2015.02.003

[31] Shimizu Y, Suda Y, Takikawa H, Ue H, Shimizu K, Umeda Y. Effective utilization of carbon nanocoil-supported PtRu anode catalyst by applying anode microporous layer for improved direct methanol fuel cell performance. Electrochemistry. 2015;**83**:381-385. DOI: 10.5796/electrochemistry.83.381

[32] Tang S, Huangfu H, Dai Z, Sui L, Zhu Z. Preparation of Fe-N-carbon nanocoils as catalyst for oxygen reduction reaction. International Journal of Electrochemical Science. 2015;**10**:12. http://www.electrochemsci.org/papers/vol10/100907180.pdf

[33] Rakhi RB, Cha D, Chen W, Alshareef HN. Electrochemical energy storage devices using electrodes incorporating carbon nanocoils and metal oxides nanoparticles. The Journal of Physical Chemistry C. 2011;**115**:14392-14399. DOI: 10.1021/jp202519e

[34] Rakhi RB, Chen W, Alshareef HN. Conducting polymer/carbon nanocoil composite electrodes for efficient supercapacitors. Journal of Materials Chemistry. 2012;**22**:5177. DOI: 10.1039/c2jm15740c

[35] Choi WH, Choi MJ, Bang JH. Nitrogen-doped carbon nanocoil array integrated on carbon nanofiber paper for supercapacitor electrodes. ACS Applied Materials & Interfaces. 2015;**7**:19370-19381. DOI: 10.1021/acsami.5b05527

[36] Izumi H, Okabe Y, Suda Y, Takikawa H, Tanoue H, Ue H, et al. Manufacturing of electric double-layer capacitors using carbon nanocoils and evaluation of their specific capacitance at a high scan rate. IEEJ Transactions on Fundamentals and Materials. 2013;**133**:660-667. DOI: 10.1541/ieejfms.133.660

[37] Yu L, Wan G, Qin Y, Wang G. Atomic layer deposition assisted fabrication of high-purity carbon nanocoil for electrochemical energy storage. Electrochimica Acta. 2018;**268**:283-294. DOI: 10.1016/j.electacta.2018.02.114

[38] Tibbetts GG. Carbon fibers produced by pyrolysis of natural gas in stainless steel tubes. Applied Physics Letters. 1983;**42**:666-668. DOI: 10.1063/1.94066

[39] Yokota M, Hosokawa Y, Shinohara Y, Kawabata T, Takimoto K, Suda Y, et al. Splitting and flattening of helical carbon nanofibers by acid treatment. Journal of Nanoscience and Nanotechnology. 2010;**10**:3910-3914. DOI: 10.1166/jnn.2010.1964

[40] Pan L, Zhang M, Nakayama Y. Growth mechanism of carbon nanocoils. Journal of Applied Physics. 2002;**91**:10058. DOI: 10.1063/1.1471575

[41] Li D, Pan L. Necessity of base fixation for helical growth of carbon nanocoils. Journal of Materials Research. 2012;**27**:431-439. DOI: 10.1557/jmr.2011.401

[42] Hirahara K, Nakayama Y. The effect of a tin oxide buffer layer for the high yield synthesis of carbon nanocoils. Carbon. 2013;**56**:264-270. DOI: 10.1016/j.carbon.2013.01.007

[43] Suda Y, Ishii Y, Miki T, Maruyama K, Tanoue H, Takikawa H, et al. Improvement of carbon nanocoil purity achieved by supplying catalyst molecules from the vapor phase in chemical vapor deposition. Journal of Materials Research. 2014;**29**:2179-2187. DOI: 10.1557/jmr.2014.247

[44] Chang N-K, Chang S-H. High-yield synthesis of carbon nanocoils on stainless steel. Carbon. 2008;**46**:1106-1109. DOI: 10.1016/j.carbon.2008.03.020

[45] Bi H, Kou K-C, Ostrikov KK, Wang Z-C. High-yield atmospheric-pressure CVD of highly-uniform carbon nanocoils using Co-P catalyst nanoparticles prepared by electroless plating. Journal of Alloys and Compounds. 2009;**484**:860-863. DOI: 10.1016/j.jallcom.2009.05.064

[46] Qi X, Zhong W, Deng Y, Au C, Du Y. Synthesis of helical carbon nanotubes, worm-like carbon nanotubes and nanocoils at 450°C and their magnetic properties. Carbon. 2010;**48**:365-376. DOI: 10.1016/j.carbon.2009.09.038

[47] Li D, Pan L, Qian J, Liu D. Highly efficient synthesis of carbon nanocoils by catalyst particles prepared by a sol-gel method. Carbon. 2010;**48**:170-175. DOI: 10.1016/j.carbon.2009.08.045

[48] Wang W, Yang K, Gaillard J, Bandaru PR, Rao AM. Rational synthesis of helically coiled carbon nanowires and nanotubes through the use of tin and indium catalysts. Advanced Materials. 2008;**20**:179-182. DOI: 10.1002/adma.200701143

[49] Cervantes-Sodi F, Vilatela JJ, Jiménez-Rodríguez JA, Reyes-Gutiérrez LG, Rosas-Meléndez S, Íñiguez-Rábago A, et al. Carbon nanotube bundles self-assembled in double helix microstructures. Carbon. 2012;**50**:3688-3693. DOI: 10.1016/j.carbon.2012.03.042

[50] Waring CE, Horton WS. The kinetics of the thermal decomposition of gaseous tetramethyltin. Journal of the American Chemical Society. 1945;**67**:540-547. DOI: 10.1021/ja01220a014

[51] Dyagileva LM, Mar'in VP, Tsyganova EI, Razuvaev GA. Reactivity of the first transition row metallocenes in thermal decomposition reaction. The Journal of Organic Chemistry. 1979;**175**:63-72. DOI: 10.1016/S0022-328X(00)82299-8

[52] Suda Y, Maruyama K, Iida T, Takikawa H, Ue H, Shimizu K, et al. High-yield synthesis of helical carbon nanofibers using iron oxide fine powder as a catalyst. Crystals. 2015;**5**:47-60. DOI: 10.3390/cryst5010047

[53] Sugioka Y, Suda Y, Tanoue H, Takikawa H, Ue H, Shimizu K, et al. Effects of dielectric barrier discharge treatment conditions on the uprightness of carbon nanofibers. IEEE Transactions on Plasma Science. 2012;**40**:1794-1800. DOI: 10.1109/TPS.2012.2199769